Tomographic study of helical modes in bifurcating Taylor-Couette-Poiseuille flow using magnetic resonance imaging

Kevin W. Moser, L. Guy Raguin, and John G. Georgiadis*
Department of Mechanical & Industrial Engineering, Bioengineering Program, University of Illinois at Urbana-Champaign, Urbana, Illinois 61801
(Received 30 January 2001; published 28 June 2001)

The quantitative visualization of flow in a wide-gap annulus (radius ratio 0.5) between concentric cylinders with the inner cylinder rotating and a superimposed axial flow reveals a novel mixed-mode state at relatively high flow rates. A fast magnetic resonance imaging sequence allows the cinematographic dissection and three-dimensional reconstruction of supercritical nonaxisymmetric modes in a regime where stationary helical and propagating toroidal vortices coexist. The findings shed light on symmetry-breaking instabilities, flow pattern selection, and their consequences for hydrodynamic mixing in a complex laminar flow that constitutes a celebrated prototype of many mixing or fractionation processes.

DOI: 10.1103/PhysRevE.64.016319 PACS number(s): 47.32.−y, 47.20.−k, 47.80.+v

I. INTRODUCTION

Following the original study by Taylor of the emergence of toroidal vortices superimposed on circular Couette flow in the annular space between two coaxial cylinders, an expansive literature and exegesis has developed on many of its variants [1]. In part because they form the basis for many mixing and/or separation processes or because they serve to define canonical problems for the study of transition to turbulence, the challenge is to study such flows in the strongly nonlinear regime and in realistic geometries. A noninvasive cinematographic magnetic resonance imaging (MRI) technique has been developed [2] for the Taylor-Couette problem with a superposed axial Poiseuille flow, hereafter referred to as the TCP flow. This study focuses on steady and unsteady hydrodynamic modes that emerge as the rotational speed of the inner cylinder and pressure-driven axial flow rate are varied. These modes constitute primary, secondary, and higher-order bifurcations, which break the symmetry of the base helical flow and represent drastic changes in the flow structure and attendant modifications of hydrodynamic mixing. The study of such bifurcations is crucial in the optimization of equipment designed for the separation or mixing of liquid-gas and liquid-solid mixtures [3–6].

The study of laminar vortical structures has been well documented in the Taylor-Couette (TC) flow for an extensive range of gap sizes [7–10]. Of particular interest are the experimentally determined boundaries in the map of flow regimes [11] where the propagating helical vortex and stationary toroidal vortex modes become stable simultaneously and interact in the presence of the $O(2)\times SO(2)$ symmetry of the TC apparatus. The bifurcation diagrams in the vicinity of such a codimension-2 point indicate the possibility for coexistence (bicriticality) of these two modes for wide-gap annuli [12,13]. This presents new opportunities to study complex nonlinear interactions at relatively low rotation rates (i.e., in the neighborhood of the primary bifurcation) in variants of the TC problem, such as TCP flow.

The flow domain of TCP flow is characterized by two geometrical parameters: the ratio of the inner cylinder radius to the outer one, $\eta=R_1/R_2$, and the ratio of the length L of the cylinders to the annulus gap width ($d=R_2-R_1$), termed the aspect ratio $\Gamma=L/d$. TCP flow is also characterized by two dimensionless dynamical parameters corresponding to the angular velocity of the inner cylinder (Ω) and the imposed mean axial velocity (U_z): the Taylor number, $\mathrm{Ta}=4d^4(\Omega/\nu)^2\eta^2/(1-\eta^2)$, and the axial Reynolds number, $\mathrm{Re}=U_z d/\nu$. The majority of the TCP studies concern primary bifurcations [14–17] or relatively narrow gaps [18,19]. However, visual [20,21] and optical [22,23] experimental studies have established the existence of various nonaxisymmetric regimes with wider gaps, as seen in Fig. 1. Motivated by the bicritical states observed in TC systems, similar behavior is also anticipated in wide-gap TCP systems. The experimental technique employed here obviates the limitations of optical diagnostics [19] or ultrasound techniques [9], which extract velocities in only a portion of a meridional plane of the annular flow.

II. EXPERIMENT

Magnetic resonance imaging (MRI) is a tomographic imaging technique that makes it possible to image arbitrary cross sections through the interior of rotating systems and to obtain information about the velocity profiles directly. One form of MRI velocimetry is spin tagging, which involves tagging nuclear spins throughout the sample. By modulating the longitudinal spin polarization in two orthogonal directions, a Cartesian grid can be formed and tracked in subsequent images. In an image acquired immediately after the tagging, the grid appears undistorted. However, the grid deforms as the tags evolve with the flow, as seen in the right panel of Fig. 2. Fluid motion between the first and subsequent images is extracted from the displacement and distortion of the grid. By acquiring images every 0.5 to 0.75 s with an ultrafast imaging technique (FLASH), direct visualization of flow patterns can be obtained in the form of cinematography [2].

*Author to whom correspondence should be addressed.

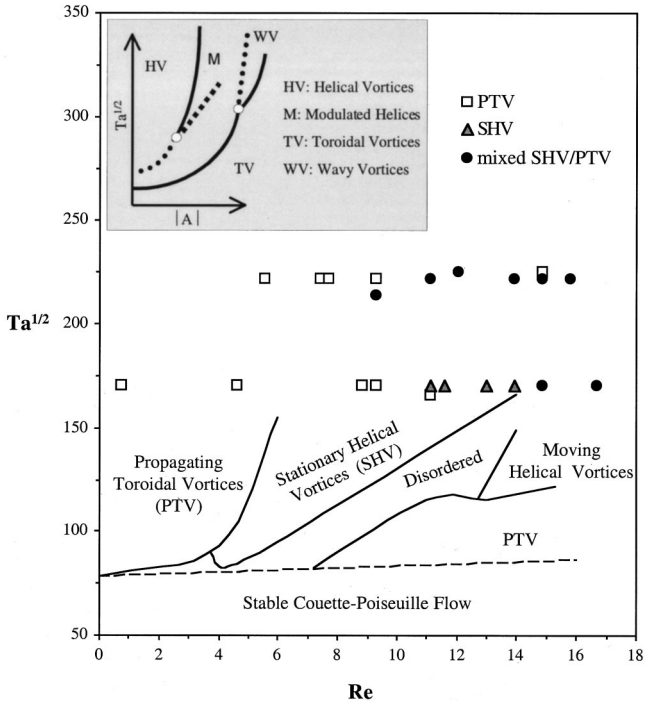

FIG. 1. Flow regimes observed in the TCP flow for $\eta=0.5$ (discrete data points) and $\eta=0.77$ (curved boundaries adapted from Ref. [23]). Also shown (inset) is the bifurcation diagram adapted from Ref. [13] for the Taylor-Couette (TC) flow. In the inset, solid lines represent stable branches and dotted lines represent unstable branches.

The measurements were performed at the University of Illinois Biomedical Magnetic Resonance Laboratory using a 4.7 T magnet with gradient capabilities up to 6.5 Gauss/cm. The system is a Varian 200/330 imaging spectrometer with Oxford ASG-26 gradients controlled via VNMR 6.1A software protocols. The rf coil used in the experiments was a 6 cm i.d. birdcage coil. The inner rotating cylinder of the test section had a radius $R_1=9.525$ mm while the fixed outer cylinder had a radius $R_2=19.05$ mm ($\eta=0.5$). To achieve uniform flow in the entrance and exit cross sections, 25.4 mm thick disks perforated with an array of 1 mm diameter channels were fixed at both ends. The useful length between these disks was $L=152$ mm, making $\Gamma\approx 16$. A more complete description and schematic of the test section can be found in [2].

III. RESULTS

The results reported here are for two angular velocities, obtained by fixing the angular velocity and increasing the axial velocity. Figure 1 shows that the qualitative aspects of the observed states are similar to those reported in the literature. As the axial flow rate increases, the base helical (Couette-Poiseuille) flow undergoes a bifurcation to a state characterized by propagating toroidal vortices (PTV), followed by stationary helical vortices (SHV) and disordered moving helices or PTV. Besides the present paper ($\eta=0.5$), SHV was observed for $\eta=0.77$ [23], $\eta=0.8$ [21], and $\eta=0.83$ [22]. SHV flow has not been studied systematically before, probably due to mode ''crowding'' in these narrow-gap systems. For $\mathrm{Ta}^{1/2}=170$ and increasing axial Reynolds numbers, the flow is first characterized by PTV, then SHV, before breaking down into mixed SHV/PTV (Fig. 1). This new TCP state is a spatial juxtaposition of SHV upstream and PTV downstream. The existence of a front separating wave patterns with different frequencies, such as that between SHV and PTV, is characteristic of driven dissipative systems in finite domains with waves traveling preferentially in one direction [24].

The three-dimensional (3D) velocity field of SHV was reconstructed by using various MRI images of the flow. The axial component of the velocity was measured from the coronal ($\theta=0,\pi$) MRI images of SHV by assuming that the flow possesses a helical symmetry so that each $U_z(r,\theta)$ profile at a z_0 location is identical to that at $z=z_0+\lambda\theta/2\pi$, where λ is the wavelength. This is confirmed by examining transverse images ($z=$const) and additional saggital ($\theta=\pi/2,3\pi/2$) MRI images. The radial and azimuthal velocity components were obtained from five transverse MRI images at locations marked in Fig. 2. The transverse images helped delineate the counter-rotating helical vortices (rendered in the left panel of Fig. 2) as they wind their way through the test section.

Examination of the cinematographic image sequences at higher axial flow rates (Fig. 3) reveals that the transition SHV→PTV is marked by convective instabilities. These are characterized by undulations of the strong outward jets (reminiscent of the ''jet modes'' of TC [10]), which interrupt the core flow of each helix and segment the corresponding vortex filaments at a given axial location. Each filament segment then closes to form a vortex ring as they advect downstream. The counter-rotating rings stack up to create the PTV pattern observed downstream, translating at axial velocities from $1.06U_z$ to $1.18U_z$. This transition is consistent with the preservation of the helical symmetry of the stationary SHV flow and will be revisited in view of the correspondence between TCP and TC bifurcations.

IV. DISCUSSION: SHV VS PTV

Important physical insights about the SHV and PTV states can be obtained by examining the ratio of the rotational to translational time scales, $R_g=\tau_{\mathrm{rot}}/\tau_{\mathrm{tran}}$. Consider a fluid particle following an ideal helical motion with constant azimuthal velocity U_θ on a cylindrical surface with radius r. The period $\tau_{\mathrm{rot}}=2\pi r/U_\theta$ to complete one revolution about the axis would match the time $\tau_{\mathrm{tran}}=\lambda/U_z$ to translate by an axial wavelength λ ($R_g=1$). From four transverse images of the SHV at $\mathrm{Ta}^{1/2}=170$, positions 2–5 on Fig. 2, the average of $U_\theta(r)/r$ for each slice was found to be 0.2309Ω with less than a 5% variation between slices. Using this average to define τ_{rot} and U_z to define τ_{tran}, Fig. 4 indicates that $R_g=1$ for the SHV mode over a range of axial flow rates. The figure also shows that the SHV part of the mixed SHV/PTV mode at $\mathrm{Ta}^{1/2}=220$ is close to unity, hence suggesting $R_g=1$ whenever the SHV mode is observed. In contrast, $R_g=1.2\,\mathrm{Re}/\mathrm{Ta}^{1/4}$ in the PTV flow regime, as seen in Fig. 4 for $\mathrm{Ta}^{1/2}=170$ and 220. These observations for SHV can be used to predict its axial wavelength for other values of Re and Ta.

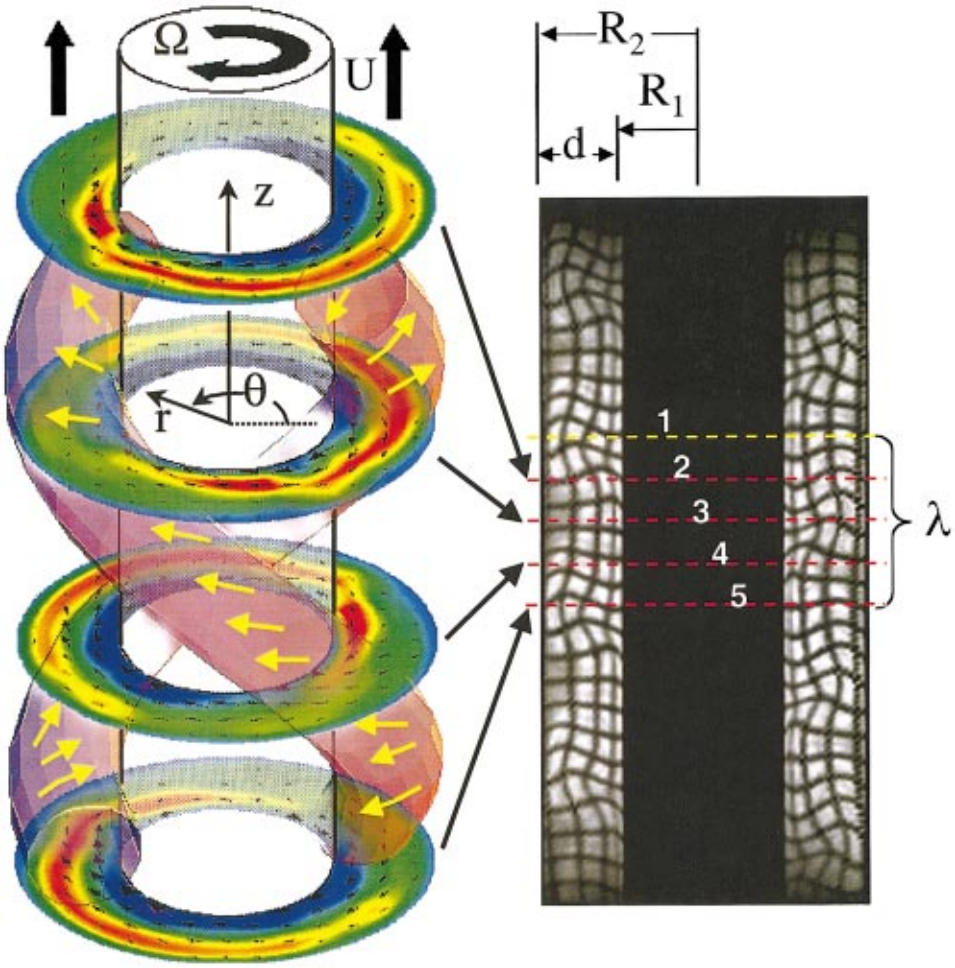

FIG. 2. (Color) Stationary helical vortex (SHV) in the TCP flow (left panel) for $Ta^{1/2}=170$ and $Re=11.14$, reconstructed by exploiting the helical symmetry of the flow and by extracting data from the coronal MRI image (right panel). Four transverse slices are rendered here with color representing the magnitude of axial (z) velocity (red: positive; blue: negative) and with superimposed transverse-plane (r-θ) velocity vectors. The skeleton of the SHV flow represented by the vortex tubes has been superimposed; the rendering follows aesthetic criteria and only means to elucidate the ''double helix'' topology.

Setting $\tau_{rot}=\tau_{tran}$ and dividing by the annulus gap width, the axial wavelength is given by

$$\frac{\lambda}{2(R_2-R_1)}=\frac{\pi U_z}{0.2309\Omega(R_2-R_1)}=15.71\frac{\mathrm{Re}}{\mathrm{Ta}^{1/2}}. \qquad (1)$$

Figure 4 strongly suggests that SHV and PTV (both nonlinear states) are linked dynamically. In the absence of a rigorous nonlinear bifurcation study of TCP flow, a heuristic approach has been pursued. The existence of a stable helical state (SHV) in TCP flow with continuous symmetry

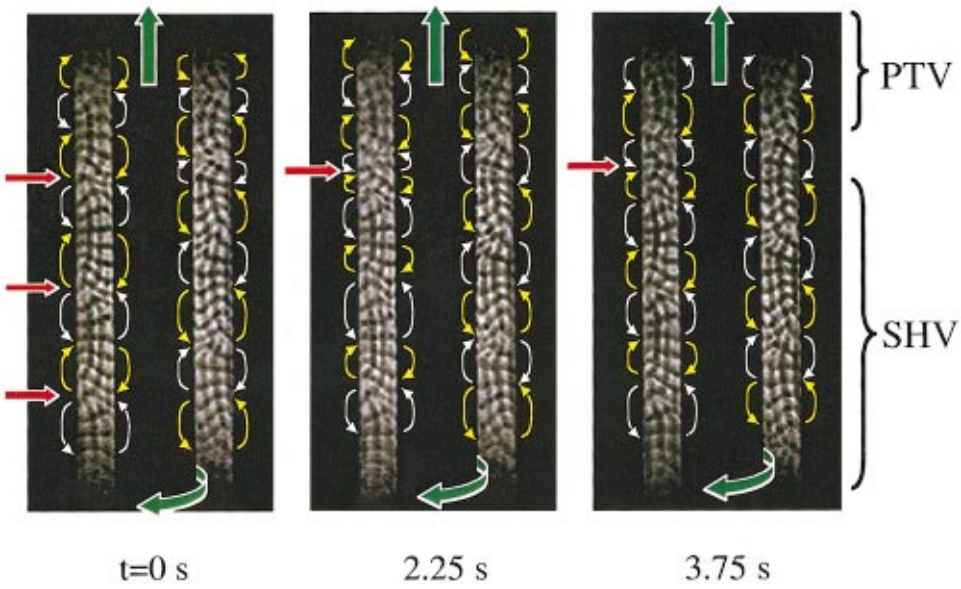

FIG. 3. (Color) Consecutive coronal MRI images of TCP flow demonstrating the evolution of the mixed SHV/PTV state for $Ta^{1/2}=220$ and $Re=14.8$. Green arrows indicate the direction of the axial flow and shaft rotation. Yellow arrows correspond to the helical vortex corotating with the inner cylinder. The topology of the counter-rotating helical vortex (white arrows) is complementary. A downstream growing undulation of the radial outward jet (marked by three red arrows at $t=0$ s) results in an ''extra'' pair of counter-rotating vortices (single red arrows at $t=2.25$ and 3.75 s) that break the helical symmetry.

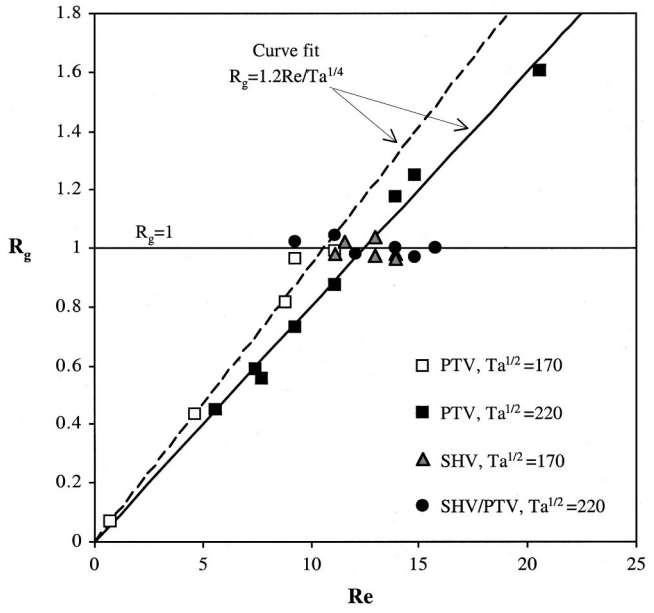

FIG. 4. Variation of the ratio of rotation to axial translation time scales, $R_g=\tau_{\mathrm{rot}}/\tau_{\mathrm{tran}}$, with the nondimensional average axial velocity, Re.

$(r,\theta,z)\rightarrow(r,\theta+\Theta,z+\lambda\Theta/2\pi)$, where θ and Θ are given in radians, motivates a search for a mapping between SHV in TCP flow and propagating helical vortices in TC flow. Langford *et al.* [12] performed a linear analysis of bicriticality in TC flow by considering the stability of modes with the form $\sim F(r)\exp[i(kz+m\theta)+\sigma^{*}t]$. A codimension-2 bifurcation was found for the case where $\eta=0.50$ with stationary toroidal vortices ($m=0$, $\sigma^{*}=0$) and propagating helical vortices ($m=1$, $\sigma^{*}=\pm i\sigma$, where $\sigma=0.2813\Omega$). In addition, a weakly nonlinear bifurcation analysis [13] indicated that the bifurcation branch corresponding to the helical vortex state is initially unstable at the primary bifurcation at $\mathrm{Ta}^{1/2}=114.42$, but becomes stable at higher values of Ta. This helical state also coexists with a toroidal vortex state at a secondary bifurcation point, where another unstable branch corresponding to modulated helical vortex state appears.

Now consider a bistable state consisting of propagating helical and stationary toroidal vortices in the TC flow under a Galilean coordinate system transformation $Z=z-Vt$. This corresponds to moving the observer with velocity V along the negative axis of the cylinders. In the z reference frame, upstream-propagating helical vortices of the form $\sim F(r)\exp[i(kZ+m\theta)+i\sigma t]$ become stationary if $V=\sigma/k$. Applying the critical value of σ for the primary bifurcation described above gives a constraint in the form

$$\frac{\lambda}{2(R_2-R_1)}=\frac{\pi V}{0.2813\Omega(R_2-R_1)}. \tag{2}$$

Furthermore, the above coordinate translation transforms the stationary Taylor vortices into toroidal vortices propagating downstream with the same axial velocity V. The mean flow in the transformed coordinate system $(z=Z+Vt)$ is analogous to the base TCP flow if the effect of the no-slip boundary conditions is ignored. The above transformation produces a uniform axial profile in the gap between the cylinders, in contrast to the near parabolic base Poiseuille profile for TCP flow. This can be considered as the inviscid approximation of the TCP flow. This difference notwithstanding, Eq. (2) is identical to the wave number selection criterion in Eq. (1) if $V=1.22U_z$, which is consistent with the propagation velocity of the toroidal vortices in TCP flow estimated from Fig. 3. It should be noted that Eq. (2) was derived for $\eta=0.50$, although a similar analysis supports the validity of this hypothesis in the narrow gap limit $\eta\rightarrow 1$.

To further probe the correspondence between the TC and TCP flows, the bifurcation diagram for the TC flow [13] has been included in the inset of Fig. 1. As oriented, the horizontal axis corresponds to the amplitude $|A|$ of the perturbation and bears no formal connection with Re in the TCP bifurcation diagram. However, an analogy can be established between the axial flow in the TCP flow (Re>0) and the counter-rotation of the outer cylinder for the TC flow: both increase the shear of the mean flow and induce stable helical modes. The propagating helix of the TC flow (corresponding to SHV for TCP flow) coexists with stationary toroidal vortices (corresponding to PTV for TCP flow). These experiments show that SHV and PTV can coexist in TCP flow with an intermediate transient pattern (corresponding to the unstable ''*M*'' state for the TC flow). Carrying this correspondence further, it becomes easier to understand why the TCP experiments exhibit hysteresis and the transition SHV→PTV (not PTV→SHV). Due to the breaking of the axial O(2) symmetry and the imposition of absorbing outflow boundary conditions, disturbances travel downstream [24] and therefore serve to increase the amplitude of perturbation.

The knowledge of the TCP flow kinematics allows the study of its mixing characteristics [25] with respect to the hydrodynamic dispersion of a passive scalar. MRI essentially adopts a Lagrangian point of view, so it can also provide a direct measure of hydrodynamic dispersion. Compared to the SHV part of the flow, there was considerable signal loss in the PTV regions that increased with Re. These losses can be attributed to a reduction of phase coherence of the MRI signal due to subvoxel mixing [26]. This implies that the effective dispersion is higher in the PTV mode versus the SHV mode. The axial nonuniformity of dispersion in the SHV/PTV state opens new opportunities in the design of process equipment. One can envision a segmented operation with fractionation upstream (e.g., by imposing an external field in the SHV part), followed by enhanced mixing downstream (in the PTV part).

V. CONCLUSIONS

The significance of this study is threefold. First, by tagging and tracking the evolution of Cartesian grids in water, MRI allows the noninvasive visualization of the 3D TCP flow via sectioning on arbitrary planes. Second, in a study of hydrodynamic instabilities, this study elucidated the spatiotemporal structures associated with flow transition during a codimension-2 bifurcation in TCP flow and provided a pat-

tern selection criterion. The correspondence between the TC flow and the TCP flow, which proved to be more than superficial, can be further exploited in the study of secondary bifurcations. Third, this study differs from others in terms of operating conditions. Higher rotational and axial speeds were used in an experimental apparatus that approximates practical flows employed in process engineering. The enhancement of mixing with PTV as opposed to the SHV is relevant to the design of mixing or fractionation devices.

ACKNOWLEDGMENTS

This project is supported by the NSF (Grant No. CTS-9521509), DARPA (Grant No. DABT63-98-C-0053), and the NIH NCRR (Grant No. PHS-5P41RR05964).

[1] R. Tagg, in *Ordered and Turbulent Patterns in Taylor-Couette Flow*, edited by C. D. Andereck and F. Hayot (Plenum Press, New York, 1992), p. 303.
[2] K. W. Moser *et al.*, Magn. Reson. Imaging **18**, 199 (2000).
[3] M. Piva *et al.*, J. Phys. III **7**, 895 (1997).
[4] R. C. Giordano *et al.*, Chem. Eng. Sci. **53**, 3635 (1998).
[5] G. A. Ameer *et al.*, Proc. Natl. Acad. Sci. U.S.A. **96**, 2350 (1999).
[6] G. Baier and M. D. Graham, Phys. Fluids **12**, 294 (2000).
[7] R. C. DiPrima and H. L. Swinney, in *Hydrodynamic Instabilities and the Transition to Turbulence*, edited by H. L. Swinney and J. P. Gollub (Springer-Verlag, Berlin, 1981), p. 139.
[8] S. T. Wereley and R. M. Lueptow, J. Fluid Mech. **364**, 59 (1998).
[9] Y. Takeda, W. E. Fischer, and J. Sakakibara, Science **263**, 502 (1994).
[10] K. Kose, Phys. Rev. Lett. **72**, 1467 (1994).
[11] C. D. Andereck, S. S. Liu, and H. L. Swinney, J. Fluid Mech. **164**, 155 (1986).
[12] W. F. Langford *et al.*, Phys. Fluids **31**, 776 (1998).
[13] M. Golubitsky and W. F. Langford, Physica D **32**, 362 (1998).
[14] D. I. Takeuchi and D. F. Jankowski, J. Fluid Mech. **102**, 101 (1981).
[15] B. S. Ng and E. R. Turner, Proc. R. Soc. London, Ser. A **382**, 83 (1982).
[16] A. Tsameret and V. Steinberg, Phys. Rev. E **49**, 1291 (1994).
[17] K. L. Babcock, G. Ahlers, and D. S. Cannell, Phys. Rev. E **50**, 3670 (1994).
[18] K. W. Schwartz, B. E. Springett, and R. J. Donnelly, J. Fluid Mech. **20**, 281 (1964).
[19] S. T. Wereley and R. M. Lueptow, Phys. Fluids **11**, 3637 (1999).
[20] H. M. Nagib, Ph.D. thesis, Illinois Institute of Technology, 1972.
[21] K. Bühler and N. Polifke, in *Nonlinear Evolution of Spatio-Temporal Structures in Dissipative Continuous Systems*, edited by F. H. Busse and L. Kramer (Plenum Press, New York, 1990), p. 21.
[22] R. M. Lueptow, A. Docter, and K. Min, Phys. Fluids A **4**, 2446 (1992).
[23] A. Tsameret and V. Steinberg, Phys. Rev. E **49**, 4077 (1994).
[24] S. M. Tobias, M. R. E. Proctor, and E. Knobloch, Physica D **113**, 43 (1998).
[25] P. Ashwin and G. P. King, J. Fluid Mech. **338**, 341 (1997).
[26] D. LeBihan *et al.*, Radiology **168**, 497 (1988).